Rev. Roum. Sci. Techn.– Électrotechn. et Énerg.
Vol. **65**, *1-2*, pp. 41–46, Bucarest, 2020

Dedicated to the memory of Academician Gleb Drăgan

IMPROVEMENT OF THE PERFORMANCES OF ELECTRIC MACHINES WITH APPLICATIONS IN AERONAUTICS, USING SPECIAL MATERIALS

CRISTINEL ILIE[1], NICOLAE TĂNASE[1], IONEL CHIRIȚĂ[1], ADRIAN NEDELCU[1], MIHAI GUȚU[1]

Key words: Double excitation, Electric generator, Cobalt alloys, Permanent magnets, Simulation, Testing.

The paper presents how the performances of an electric microgenerator with double excitation used in aeronautical applications have been improved, using special materials, with superior characteristics. Thus, if the usual ferromagnetic materials were used in the initial model, in the improved model, a modern ferromagnetic material was chosen, with superior magnetic characteristics, Supermendur (HiperCo 50), massive core for the inductor and lamination sheets for the armature. For the parts that do not have a role in the magnetic circuit of the electric machine, there has been used a synthetic material, Ketron, material with higher mechanical characteristics but with low specific weight, at the same time, minimizing the interior spaces. Finally, this paper presents comparatively the electrical characteristics for the two electric machines, the one manufactured with usual, classic materials (OL37 iron and FeSi #0.2mm for the laminations sheets), and the other one with special materials as HiperCo 50. The manufacturing technology is presented briefly for some of the parts.

1. INTRODUCTION

Benefiting from globally supported R&D programs (USA, EU, ASIA) in both the military and civilian fields, unmanned aerial vehicles (UAVs) have reached an unprecedented level of development. This type of aircraft has become indispensable in modern conflicts and it is expected to soon take the lead on the battlefield. If at the beginning the use of UAVs was exclusively military (in surveillance, detection, classification, identification, tracking and neutralization missions), now they have a wide use, also in the civilian field (agriculture, infrastructure, transport, cinema) [1–3].

In order to be able to offer a greater autonomy of flight, the companies involved in this field try to develop propulsion systems - thermal or electric motors - as efficient as possible and with the lowest possible costs [4–6].

For UAV systems equipped with both thermal and electric propulsion (hybrid propulsion), it is very important to develop electric generators with superior performance. They must have as much power as possible and a weight as small as possible, to maximize the payload of the UAV system [7–10].

Thus, an electric generator was created for a UAV system with hybrid propulsion; the authors opted for a synchronous variant with excitation by permanent magnets, according to their own idea "with double excitation"; besides, this solution has been patented [11, 12].

This design, in a single-phase synchronous version, has the armature fixed, in the shape of an empty cylinder, made from laminations, on which the copper conductors are wire wound and the inductor (rotor) is double, with two concentric consolidated yokes having cylindrical sections, flanking bilaterally the armature, externally and internally.

This design differs from the classic electric machines because it has the coils are on both sides stator (toroidal winding on the ring-shape stack of lamination) active both at the external and internal air gap, located in the hetero-polar magnetic field being generated by the outer inductor respectively the inner inductor, made with permanent magnets, solidified on the double rotor.

A higher specific power of the electric machine is obtained, due to the fact that the electromotive forces that appear in the coils, due to both interactions with inside and outside permanent magnets, are gathering.

There were manufactured two constructive models, identical in terms of the size, dimensions, the number of poles and the characteristics of the permanent magnets. Usual ferromagnetic materials were used for the first model; for the improved electric generator, special ferromagnetic materials with superior characteristics were used.

2. THE CONSTRUCTIVE SOLUTION

For both variants of the electric machines, the constructive solution is similar and is presented in Fig. 1.

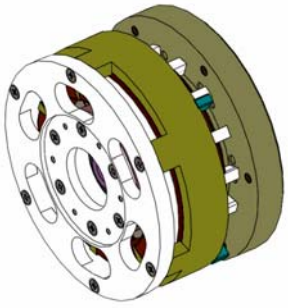

a) General assembly of the generator

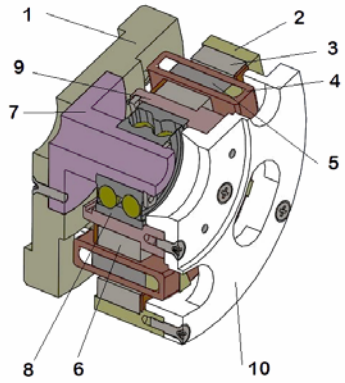

b) Cross section of the generator

Fig. 1 – Constructive solution for electric generator with double excitation (1 – lower flange; 2 – outer yoke and case; 3 – outer magnets; 4 – winding; 5 – laminations; 6 – inner magnets; 7 – axle; 8 – ball bearing; 9 – inner yoke; 10 – superior flange).

[1] National Institute for R&D in Electrical Engineering ICPE-CA, Bucharest, 030138, Romania, E-mail: cristinel.ilie@icpe-ca.ro

From Fig. 1 it can be seen the stator subassembly that has a lower flange {1} with which it is attached to the place of operation. On this flange is fixed, with special clamps, the laminations stack (the stator made of FeSi or HiperCo 50), reinforced by soldering {5}.

The stator is flanked at the front by two insulating rings with housings for the distributed coils {4}. Coaxial with the stator and flange {1}, an axle {7} is fixed and it supports the ball bearing {8} centered on the inner yoke {9}. The electric machine works with a single radial-axial bearing, with two rows of balls.

The rotor subassembly consists of the upper flange {10}, on which two concentric ferromagnetic rings are fixed, made from steel or HiperCo 50 (2 and 9).

They act as yokes for closing the magnetic flux, on which the permanent magnets are fixed, on the outer yoke to the inside {3} and on the inner yoke to the outside {6}.

The magnets, which are positioned face to face, are magnetized in opposite directions, in such a way that the hetero-polar magnetic circuit of the electric machine closes between the magnets, the lamination stack of sheets (stator) and yokes (rotor), as shown in Fig. 2 [13–15].

The main differences realized between the two variants of the electric generators in order to maximize the performances, are the following:

A. Intervention on ferromagnetic materials

The materials used for the yokes of closing the magnetic circuit at the level of the inductor and the armature where considered.

In the initial experimental model these yokes were made of conventional ferromagnetic materials, massive core using OL37 iron for the inductor (for outer and inner rings that are equipped with permanent magnets) and FeSi lamination sheets, with thickness 0.2 mm, for armature (stator).

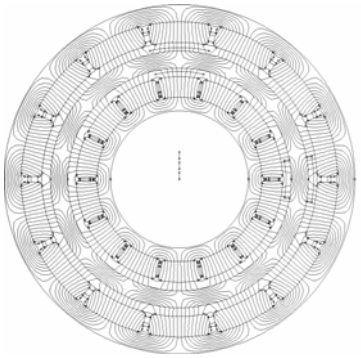

Fig. 2 – Structure of the hetero-polar magnetic field.

For the new generator model, in order to minimize the cross sections of the armatures (and lower the overall weight) but with increased magnetic stress, we opted for a modern ferromagnetic material with superior magnetic characteristics, Supermendur (HiperCo 50), both bulk for the inductor and lamination sheets metal for the armature.

Table 1

The main characteristics of HiperCo 50

Variable	Magnetic properties
Saturation induction	2.37 T
Remanent induction	1.58 T
The coercive field	98.5 A/m
Induction field at 2 T	800 A/m

Table 1 presents the main characteristics of HiperCo 50, as declared by the manufacturer [16].

We emphasize that for the generator model 2 the costs are considerably higher, due to the higher purchase price of the HiperCo 50 compared to the OL 37 iron, and due to the heat treatment to which the final parts, manufactured from HiperCo 50, must be subjected.

According to the manufacturer's specifications, the parts made from special material Hiperco 50 must be subjected to a specific heat treatment, in the atmosphere of H_2, to obtain the specified magnetic performance, according to [17, 18].

The high saturation induction level allows a 20 % reduction of the yokes sections, having the effect not only of reducing the overall weight of the assembly, but also increase the size of the outer and inner air gaps, thus being able to adopt a larger diameter of copper wire for the coils that are made around the annular armature (0.95 mm instead of 0.85 mm).

B. Intervention on the materials of the resistance and insulation structure

Based on the experience with the manufacturing and experimentation of the first model, we extended the use of the synthetic material Ketron to parts that do not play a role in the machine's magnetic circuit, minimizing the amount of metal and, at the same time, minimizing interior spaces.

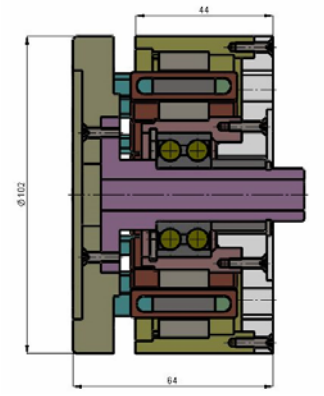

a) Initial model [15]

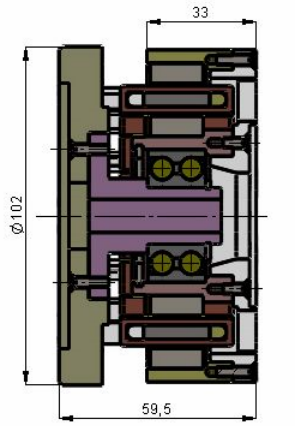

b) Improved model

Fig. 3 — General assembly of the two models for the electric generator with double excitation.

We remind that Ketron has specific weight ρ = 1.31g/cm^3, approximately 2.5 times lighter as aluminum,

but with superior mechanical properties [19]. These modifications are illustrated in the drawings of the assembly in longitudinal section for the two variants, shown in Fig. 3. It can be seen a clearly improvement of the new model regarding the overall dimensions that conduct to a much lighter micro-generator, which is important for UAV systems.

3. PERFORMANCE MAXIMIZING EFFECTS

From an overall constructive-dimensional point of view, there were no significant changes due to the improvements made and presented above. As shown in Fig. 3, in the new improved model the axial length decreases from 64 mm to 59.5 mm, that means by about 7 %, but the axial length of the armature decreases from 44 mm to 33 mm. Regarding the mass of the assembly, it decreases by about 22 %, from 1.83 kg to 1.45 kg, which is very important for aeronautical applications.

Regarding the magnetic stresses, the FEMM 4.2 [20] software was used to perform the numerical modelling and simulation for the considered electric machine, for the two constructive models.

Due to the symmetries, the model of the electric machine can be reduced to 2D problem, which substantially reduces the computation time and memory requirement [21–23]. The working regime was magneto-static, defined by:

$$\nabla \times \left(\frac{\nabla \times \mathbf{A}}{\mu(B)} \right) = \mathbf{J}, \tag{1}$$

where **A** [Wb/m] is the vector magnetic potential, **J** [A/m^2] the current density (perpendicular to the plane), and $\mu(B)$ [H/m] the magnetic permeability defined by curves *B*-*H*, for nonlinear problems.

For the boundary conditions, under the assumption that the magnetic permeability of the yokes is much higher than the air, the magnetic flux leak outside the electric machine is considered negligible, so the *Dirichlet* condition can be used:

$$\mathbf{A} = 0. \tag{2}$$

It was used a mesh network with triangular elements, with a maximum size of 0.5 mm, resulting in approximately 131,000 nodes. The solution was interpolated linearly between nodes.

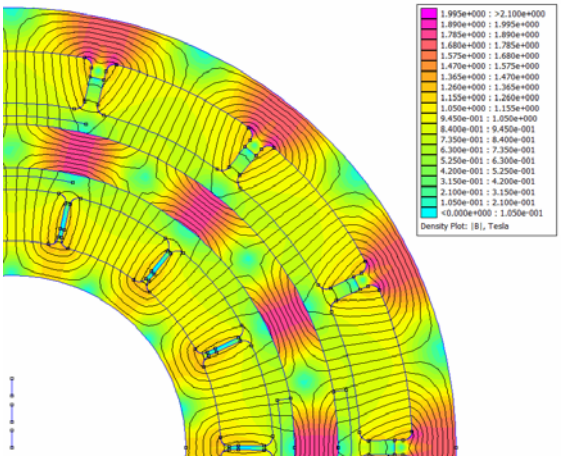

a) Magnetic flux density chart and magnetic flux lines for model 1 $|B|_{max} = 1.8$ T [15];

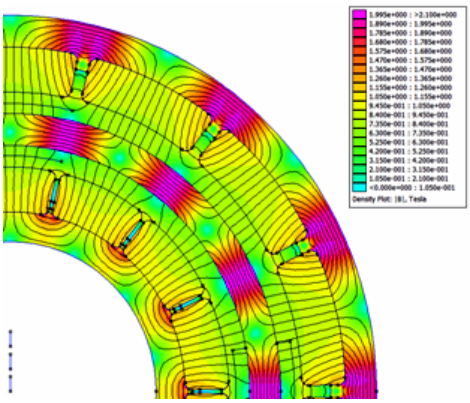

b) Magnetic flux density chart and magnetic flux lines for model 2 $|B|_{max} = 2.1$ T.

Fig. 4 – The distribution of the magnetic field lines in the two variants.

There were taken into account two materials for the magnetic yokes, FeSi sheets (armature) and OL 37 steel (rotor rings) for variant 1, and HiperCo 50 for variant 2. Both variants used NdFeB type N40SH, 40 MGOe permanent magnets.

In Fig. 4 a) and b) the solution of the magneto-static problem is presented for the two constructive models, in the form of a colored chart of magnetic flux density module |B| with overlapping of the magnetic flux lines.

In Fig. 5 a) and c) one can visualize the normal (useful) component of the magnetic flux density, $\mathbf{B}_n$, in the two air gaps, along a pole of the electric machine, for the constructive model 1, and in Fig. 5 b) and d), for the constructive model 2.

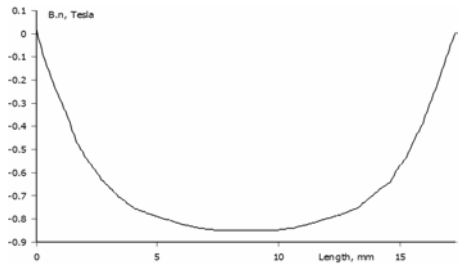

a) B_n in external air gap, model 1

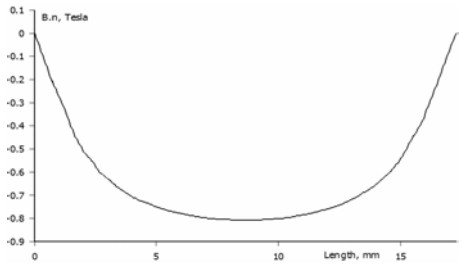

b) B_n in external air gap, model 2

c) B_n in internal air gap, model 1

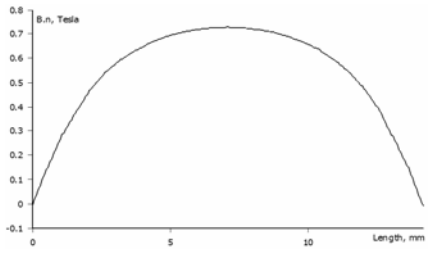

d) B_n in internal air gap, model 2.

Fig. 5 – The magnetic flux density variation on polar step for the two models.

Both variants had been designed so that the normal component results in approximately the same amplitude. The model 2, that uses the HiperCo 50 material, Fig. 6 b) with higher permeability than FeSi, Fig. 6 a) allowed a higher density of the magnetic flux density in yokes (2.1 T compared to 1.8 T) resulting in a reduction of approximately 13 % in the volume of the yokes material.

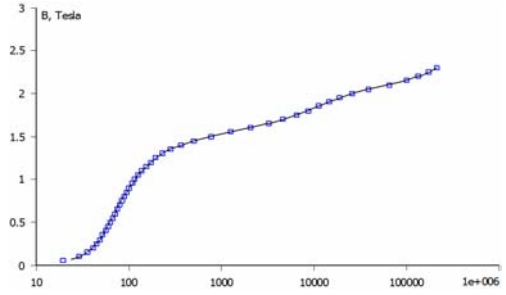

a) First magnetization curve for *Silicon Iron / M-36 Steel (FeSi)*

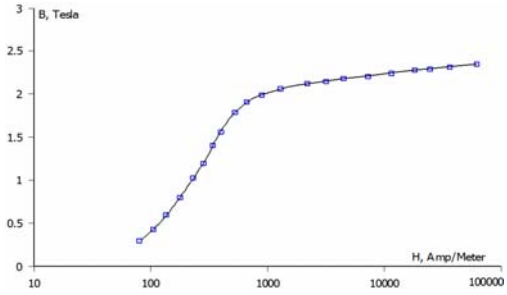

b) First magnetization curve for Cobalt Iron / Hiperco-50 (CoFe)

Fig. 6 – The first magnetization curve for the materials used for the two models.

With the values of the quantities taken from these representation, we predetermined by calculation the main characteristic parameters of the micro-generator in the two variants.

In connection with these we specify the following:

a) calculating by integration the area delimited by the induction curves, respectively the magnetic flux on the unit of axial length and referring to the maximum induction on the polar step level, we determined the coefficients *"*α_i*"* of polar coverage for the two air gaps;

b) the coils of the ring armature are in number of 2p (Fig. 7) and contains two layers of conductors type ET2-200, produced by HELENIC CABLES SA; the adjacent arrangement of the conductors at the height of the ring armature determines the phasor addition of the electromotive forces induced in the conductors from the active sides in the two air gaps, so we considered two coefficients of conductor distribution, k_{rep} (corresponding to the active sides of the two air gaps);

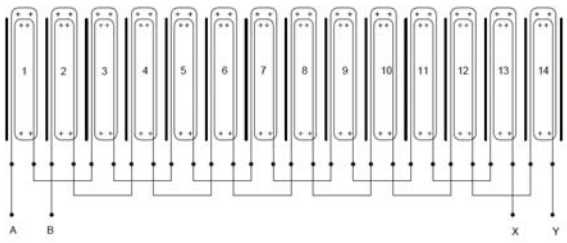

Fig. 7 — Winding scheme consisting of 14 coils arranged two by two.

c) starting from the computational relation of the instantaneous electromotive forces at the extremities of a conductor (v*B_δ*l, where v - tangential velocity, l - active axial length, equal to that of permanent magnets, B_δ – magnetic flux density in the air gap) and taking into account by the polar coating (α_i), Bz the maximum induction level ($B_{\delta max}$) in the two air gaps, as well as by the distribution of conductors (k_{rep}), we calculated the effective value of the electromotive forces (fundamental harmonic) at the ends of a coil and respectively at the terminals for connecting the coils in a series-parallel arrangement (two current paths in parallel with p coils each);

d) in order to calculate the electrical resistance of the coils, we took into account a rectangular coil end.

In Tables 2 – 4 we present the comparative results for the two micro-generator variants.

Table 2 presents the constructive data for the two micro-generators models.

Table 2

Constructive data for the two micro-generators

Measurement Unit	Model 1	Model 2
Number of pole pairs, p	7	7
Active axial length, l [mm]	16	16
Average reference diameter in the outer air gap, D_{mede} [mm]	77.5	77.5
Average reference diameter in the inner air gap, D_{medi} [mm]	62.5	62.5
Inductor yoke thickness [mm] outer ring	5	4
Inductor yoke thickness [mm] inner ring	4	4
Induced yoke thickness (sheet metal ring) [mm]	5	4.25
Diameter of the winding conductor, d_c [mm]	0.85	0.95
Number of conductors per layer	12	12
Number of layers	2	2

Regarding the comparative results of the numerical simulations for the two micro-generator models, these are shown in Table 3.

Table 3

Comparative results for numerical simulations

Measurement Unit	Model 1	Model 2
Magnetic flux on the pole and axial depth of 1 mm, Φ_{pole} [Wb], in the outer air gap	$11.39*10^{-6}$	$10.8*10^{-6}$
Magnetic induction in the outer air gap, $B_{\delta maxe}$ [T]	0.84	0.83
Magnetic flux on the pole and axial depth of 1 mm, Φ_{poli} [Wb], in the inner air gap	$8.03*10^{-6}$	$7.6*10^{-6}$
Magnetic induction in the inner air gap, $B_{\delta maxi}$ [T]	0.775	0.74

Table 4 presents the comparative results determined by

analytical calculation for the two micro-generator models.

Table 4

Comparative results for the two variants of electric generators (values determined by analytical computation)

Measurement Unit	Model 1	Model 2
Polar pitch on the reference diameter in the outer air gap, ζe [mm]	17.39	17.39
Polar pitch on the reference diameter in the inner air gap, ζi [mm]	14.025	14.025
Polar coverage factor in the outer air gap, α_{ie}	0.78	0.75
Polar coverage factor in the inner air gap, α_{ii}	0.74	0.73
Partition coefficient in the outer air gap k_{repe}	0.86	0.83
Measurement Unit	**Model 1**	**Model 2**
Partition coefficient in the inner air gap k_{repi}	0.80	0.76
Electromotive force on the coil (effective for fundamental harmonics), U_{eb} [V]	4.0	3.68
Electromotive force at the terminals (effective value for fundamental harmonics), U_e [V]	56	51.52
Electrical resistance at terminals, R_b [Ω]	0.21	0.17
Output power (active) [W] preliminary to reference speed n = 2,500 rpm and the reference current density J = 8.5A/mm^2	250	285
Output power (active) [W] preliminary to reference speed n = 2,500 rpm and the reference current density J = 10 A/mm^2	289	332

From Table 4 (the preliminary calculations) it can be observed that the output power is increased for the new improved model by about 15 %.

4. TESTING OF THE MICROGENERATOR WITH DOUBLE EXCITATION

The testing experiments of the two micro-generators include experimental tests performed in both situations, with and without load operation.

For the experimental testing with no load, the micro-generators was fixed in the presented supporting infrastructure and powered by a dc electric machine with disc rotor, with suitable power and speed (1,000 W / 3,000 rpm), Fig. 8.

a) Model 1 (V1) [15]

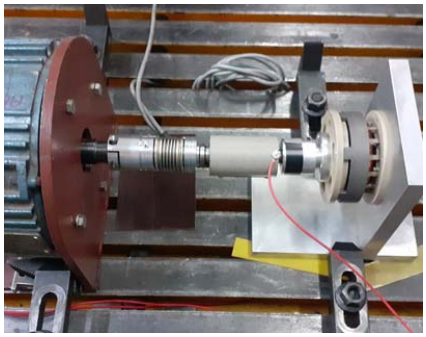

b) Model 2 (V2)

Fig. 8 – No load testing of the micro-generator.

The voltage for no load testing of the generator was obtained and it was U_1 = 47 V at model 1 and U_2 = 42.7 V for model 2, at n = 2,500 rpm speed, with current routes in series connection.

The rotation speed was measured with a tachometer type DT1236L - 10...99,999 rpm 0.1 rpm ± 0.05 %, Lutron. The voltage was measured with a digital multimeter type DMM4050 from Tektronix.

The micro-generator was powered by a dc electric machine, controlled by a voltage converter, the motion was transmitted using an elastic coupling and for torque measurement was used a mechanical torque transducer. The scheme of the load test assembly is shown in Fig. 9.

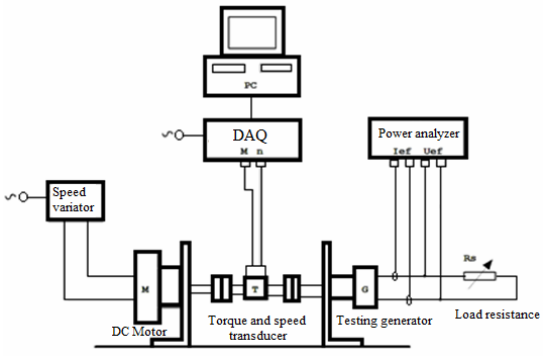

Fig. 9 – The experimental stand scheme.

To perform the load test of the generator, were used power coiled resistors with a value of 2 Ω and 1 kW power, configuring various values of resistive loads, from 2…20 Ω.

Following the processing of the results of the performed load tests, the main characteristics of the two variants of electric generator were plotted, for each coils connection variants: series and parallel of the two current routes.

The variant with serial connection has been proven to be more favorable (output power vs current density at 2,500 rpm). For this variant we present the variation curve of the output power depending on the current load at the constant rotation speed of 2,500 rpm, for the two models of the electric generator, in Fig. 10.

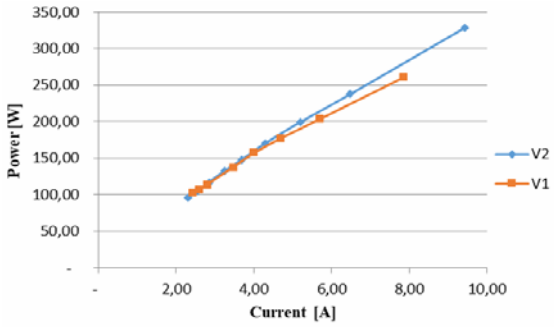

Fig. 10 – Output power depending on the output current.

In the variant 1 (V1) model, the obtained output power was 261 W, for a current measured of 7.87 A, and for the variant 2 (V2) model it was 328.8 W for a current of 9.45 A. In the following, for the variant with serial connection, the graph of the efficiency of the micro-generator was plotted according of the output power, for the two constructive models at the constant rotation speed of 2500 rpm, which is shown in Fig. 11. In the variant 1 (V1) model a maximum efficiency of 55 % was obtained and the

maximum output power was 275 W [15], at the rotation speed of 2,500 rpm. For the variant 2 (V2) constructive model, a maximum efficiency of 84 % was obtained and the maximum power was 328.8 W, at the rotation speed of 2500 rpm.

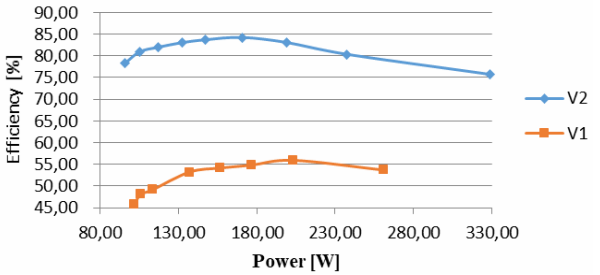

Fig. 11 – Efficiency of the generator depending on the output power.

Also for the micro-generator with serial connection, the graph of the output power was plotted according to the rotation speed, for the two constructive models, for a constant resistive load of 4 Ω. The comparative results are shown in Fig. 12.

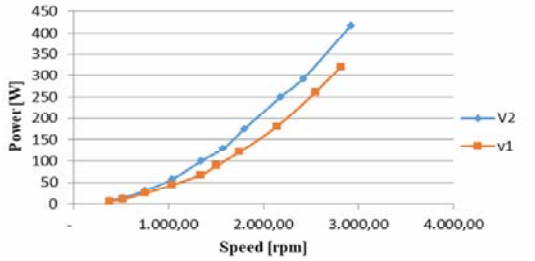

Fig. 12 – Output power vs. operating speed for a 4 Ω constant resistive load.

For the variant 1 (V1) construction model, an output power of 320 W was obtained at a speed of 2,816 rpm, and for the variant 2 (V2) model an output power of 417.7 W was obtained at a speed of 2,916 rpm.

5. CONCLUSIONS

The paper presents the efforts made to improve the performance and the obtained results for the development of a low power electric generator for an UAV platform. It should be noticed that these applications require maximum performance of the components in given conditions of size and mass, even if the costs are higher.

The improvements were mainly focused to use – for the ferromagnetic yokes that close the magnetic circuit – a special material with outstanding performance *Supermendur*, compatible with higher magnetic demands than conventional materials (soft magnetic steels, FeSi laminations sheets). These improvements have led to the possibility of the size reduction sections of the armatures, increasing the level of compaction of the construction and increasing the section of the coils conductors. Specifically, the changes finally led, for almost the same dimensional conditions, to an overall mass reduction by about 20 % and an increase in converted power (from mechanical to electrical) by about 25 %, from 261 W to 328 W and increasing efficiency from 55 % to 85 %, *i.e.*, by almost 50 %. Also it is observed, regarding the output power, that the values obtained by analytical calculation are closer to those obtained experimentally, when materials with superior characteristics are used.

ACKNOWLEDGEMENTS

The authors acknowledge the support offered through the 1SOL/2017 research grant – *Unmanned aerial platforms (UAVs) with dedicated capabilities and support infrastructure for national security mission applications*.

Received on June 9, 2020

REFERENCES

1. H. Shakhatreh , A. H. Sawalmeh, A. Al-Fuqaha, Z. Dou, E. Almaita, I. Khalil, N. S. Othman, A. Khreishah, M. Guizani, *Unmanned Aerial Vehicles (UAVs): A Survey on Civil Applications and Key Research Challenges*, IEEE Access J., **7**, pp. 48572–48634 (2019).
2. K. Alpaslan Demir, H. Cicibas, and N. Arica, *Unmanned Aerial Vehicle Domain: Areas of Research*, Defence Science Journal, **65**, *4*, pp. 319-329 (2015).
3. K. Alkaabi and A. Abuelgasim, *Applications of Unmanned Aerial Vehicle (UAV) Technology for Research and Education in UAE*, International Journal of Social Sciences Arts and Humanities, Alkaabi & Abuelgasim, **5**, *1* (2017).
4. M. Adamski, *Analysis of Propulsion Systems of Unmanned Aerial Vehicles*, Polish Air Force Academy, pp. 291-297, Dęblin, Poland, 2017.
5. M. K. Mohamed, S. Patra, A. Lanzon, *Designing Electric Propulsion System for UAVs*, Towards Autonomous Robotic Systems – 12th Annual Conference, TAROS, Sheffield, UK, 2011.
6. C. Griffis, T. Wilson, J. Schneider, P. Pierpont, *Unmanned Aircraft System Propulsion Systems Technology Survey*, U.S. Department of Transportation Federal Aviation Administration, National Technical Information Service (NTIS), Springfield, Virginia 22161, 2009.
7. P. Getsov, R. Yanev, W. Bo, *Electric motor-generators for unmanned aerial vehicles*, Aerospace Research in Bulgaria, **30**, pp 123-133, Sofia, 2018.
8. R. Capata, L. Marino, E. Sciubba, *A hybrid propulsion system for a high-endurance UAV: configuration selection, aerodynamic study, and gas turbine bench tests*, J. Unmanned Veh. Syst., **2**, pp. 17-35 (2014).
9. L. Boggero, S. Corpino, A. De Martin, G. Evangelista, M. Fioriti, M. Sorli, *A Virtual Test Bench of a Parallel Hybrid Propulsion System for UAVs*, Aerospace, **6**, *7*, 77 p. (2019).
10. S. Wang, J.T. Economou, A. Tsourdos, *Indirect engine sizing via distributed hybrid-electric unmanned aerial vehicle state-of-charge-based parametrisation criteria*, Journal of Aerospace Engineering, **233**, *14*, pp. 5360-5368 (2019).
11. G. Mihăiescu, *Contribuţii la studiul şi realizarea unor sisteme speciale cu magneţi permanenţi,* Teză de doctorat, UPB, Facultatea de Inginerie Electrică, Bucureşti, 2007.
12. Kappel W., Gavrila H., Mihaiescu G.M., Nicolaie S., Ionita V., Marin D., *Generator electric cu dubla excitatie*, Brevet nr.125881/2011.
13. A. Timotin, V. Hortopan, A. Ifrim, M. Preda, *Bazele electrotehnicii* Edit. Didactică şi Pedagocică, Bucureşti, 1970, pp. 267-314.
14. C. Ilie, G. Mihaiescu, I. Chirita, M. Gutu, M. Popa, N. Tanase, *Synchronous Electric Generator with Double Excitation*, ATEE, Electronic, pp. 1-4, Bucharest, 2019.
15. C. Ilie, N. Tănase, G. Mihăiescu, I. Chiriţă, M. Guţu, M. Popa, *Micromaşini electrice sincrone în construcţie „dublu excitată" dezvoltate la INCDIE ICPE-CA*, SME'19, Bucureşti (2019).
16. *** https://edfagan.com/hiperco-50-coil.php.
17. ***Xi`an Gangyan Special Alloy Co., Ltd., *Certificat of Analysis ASTM A801 R30005*.
18. ***Xi`an Gangyan Special Alloy Co., Ltd., *Certificat of Analysis GB/T15002-94*.
19. *** https://www.edplastics.co.uk/KETRON%20PEEK.htm.
20. *** http://www.femm.info/wiki/HomePage.
21. I. Ionică, M. Modreanu, A. Morega, C. Boboc, *Numerical Analysis of a Hybrid Stepper Motor for the Electromagnetic Torque Calculation*, 11th International Symposium on Advanced Topics in Electrical Engineering (ATEE), pp. 1-6, Bucharest, Romania, 2019.
22. V. Fireţeanu, *Analiza în element finit în studiul maşinilor electrice*, Edit. Printech, Bucureşti, 2010.
23. C.I. Mocanu, *Teoria câmpului electromagnetic,* Ed. Didactică şi Pedagogică, Bucureşti, 1982.